U.S. DEPARTMENT OF ENERGY | Office of Science

DOE/SC-CM-23-002

FY 2023 Second Quarter Performance Metric: Improving Simulations of Atmospheric Rivers and Heat Waves Using a Hierarchy of Models for High-Resolution Modeling

Paul Ullrich
Melissa Bukovskyl
Bryce E. Harrop
L. Ruby Leung

April 2023

DISCLAIMER

Contents

Figures

1.0 Product Definition

High-resolution climate data products are needed to develop a comprehensive understanding of weather and climate hazards in the Western U.S., both as they occurred historically and as they may occur in the future. Investments by the U.S. Department of Energy in global and regional climate modeling capabilities have provided new means to simulate these hazards and quantify their characteristics. In particular, the regionally refined modeling (RRM) capability in the Energy Exascale Earth System Model (E3SM) enables better resolution of the rough topography of the U.S. West, which in turn allows E3SM to better capture the impact of topography on local meteorology and associated extremes. The dynamical downscaling method (DDM), a technique that uses a secondary regional climate model forced at its boundaries, is another means to provide locally relevant climate data and better simulate extreme weather. As demonstrated in this report, these two simulation strategies can also be used together for cross-validation or to assess regional structural uncertainties via a hierarchy of models.

Atmospheric rivers (ARs) and heat waves (HWs) are two prominent meteorological features that are sensitive to changes in the broader Earth system. ARs are long, narrow bands of atmospheric moisture transport that are responsible for the majority of extreme precipitation events in the western U.S. Consequently, an understanding of ARs is important for assessing flood risk and estimating water availability. HWs are periods of sustained high near-surface temperatures that pose significant risk for human populations, ecosystems, and agriculture. Future projections for both extremes, drawn from climate models, are necessary for quantifying risk and informing relevant practitioners.

In the previous quarterly report, the performance of E3SMv1 in its low-resolution (LR) and high-resolution (HR) configurations was examined for ARs and HWs in the western U.S. In this report, we examine model performance for ARs and HWs in the western U.S. when simulations are conducted using E3SM version 2 in its regionally refined mode, and when simulations are performed using the dynamical downscaling method with the Weather Research and Forecasting (WRF) model. Results are compared with the LR configuration of E3SMv2 (LRv2) and against the European Center for Medium-Range Weather Forecasts (ECMWF) version 5 reanalysis (ERA5). Both RRM and DDM enable higher resolution over regions of interest, and hence are suitable for studies on regional weather and climate.

The evaluation of ARs and HWs in the RRM, DDM, and LRv2 simulations reveals that several key metrics show improvement when the model resolution is increased from 1 degree to 0.25 degrees, whether through regional refinement or dynamical downscaling. AR frequency and landfalling AR precipitation are both substantially improved in RRM and DDM simulations. For HWs the RRM configuration exhibits modest improvements over the LRv2 configuration, in large part due to better resolution of topography in the Western U.S. HW improvements in the DDM configuration are largely limited to HW intensity and duration, with most improvement concentrated along the coast. This difference is likely due to a cold bias in the DDM simulation, which could be ameliorated through the use of a different land model. Despite the improvements mentioned above, other metrics show little variation across the three simulations. Some of these errors may be related to biases within ERA5, which could merit further study.

2.0 Product Documentation

This report analyzes results from E3SMv2 in its RRM configuration and the WRF model, which is run using the dynamical downscaling method (DDM) and forced by E3SMv2-RRM data. E3SMv2-RRM is a global fully coupled modeling system that supports spatially variable grid spacing. The WRF model, in conjunction with NoahMP land surface model, is a regional atmosphere-land model that requires specification of meteorological fields along the domain boundary, and sea-surface temperatures at the atmosphere-ocean interface. For this study, we use the North America x4 grid, which has grid spacing of approximately 0.25 degree over and around the North American continent, and 1-degree grid spacing elsewhere. The chosen WRF grid has 0.25-degree grid spacing that extends from the western United States across much of the northeastern Pacific. The RRM and DDM grids used in this study are depicted in Figure 1. For comparison, an E3SMv2 simulation is also performed with 1-degree grid spacing (i.e., low resolution) over the entire globe, referred to as LRv2. This simulation is configured identically to the RRM simulation.

E3SMv2 simulations (both RRM and LRv2) are performed with active atmosphere, land, ocean, sea-ice, and river components. The non-hydrostatic, compressible atmosphere model is described by Rasch et al. (2019) and makes use of a 72-level spectral element dynamical core to solve the primitive equations (Dennis et al. 2012, Taylor et al. 2020). Parameterized processes include deep convection (Neale et al. 2008; Richter and Rasch 2008, Zhang and McFarlane 1995); macrophysics, turbulence, and shallow convection (Golaz et al. 2002, Larson 2017, Larson and Golaz 2005); microphysics (Gettelman and Morrison 2015, Gettelman et al. 2015); aerosol treatment (Liu et al. 2016, Wang et al. 2020); and radiative transfer (Iacono et al. 2008, Mlawer et al. 1997). The ocean and sea-ice models use the Model for Prediction Across Scales (Petersen et al. 2019, Ringler et al. 2013), and a mesoscale eddy parameterization (Gent and Mcwilliams 1990) is used for E3SM-LR only. The land model is based on the Community Land Model version 4.5 (Oleson et al. 2013), run with satellite phenology. The river model is the Model for Scale Adaptive River Transport (Li et al. 2013, 2015), using runoff simulated by the land model to compute channel velocity, channel water depth, and water surface area.

The WRFv3.9.1 simulation, in the configuration used for this report, is performed with active atmosphere, land-surface, and lake components (Skamarock et al. 2008). The atmosphere is non-hydrostatic, compressible, and was configured with 36 vertical levels, spectral nudging of wavelengths greater than ~700km, and a model top at 20hPa. Forcing data for the atmosphere (lateral boundary conditions and input for spectral nudging) comes from the E3SMv2-RRM simulation. The atmosphere grid is configured to have an approximate grid spacing of 28km. In this configuration, parameterized processes include deep convection (Kain 2004), microphysics (Hong et al. 2004), longwave (Mlawer et al. 1997) and shortwave (Chou and Suarez 1994) radiative transfer, and surface and planetary boundary-layer processes (Janjic 1994). The land-surface model is NoahMP, using TOPMODEL for runoff and groundwater, a single-layer, three-category urban canopy model, and the Community Land Model version 4.5 lake model (Niu et al. 2011, Subin et al. 2012). Ocean surface lower boundary conditions were taken from the E3SM-RRM run, and sea ice was set to form when sea surface temperatures reached a threshold of 272K or less.

For reference, the ERA5 data set (Hersbach et al. 2020) is used. ERA5 is the fifth-generation ECMWF reanalysis product, produced through assimilation of observations (e.g., aircraft, in situ, and

satellite) into the Integrated Forecasting System (IFS). ERA5 provides hourly meteorological variables on a regular 0.25-degrees latitude-longitude grid with 137 vertical levels.

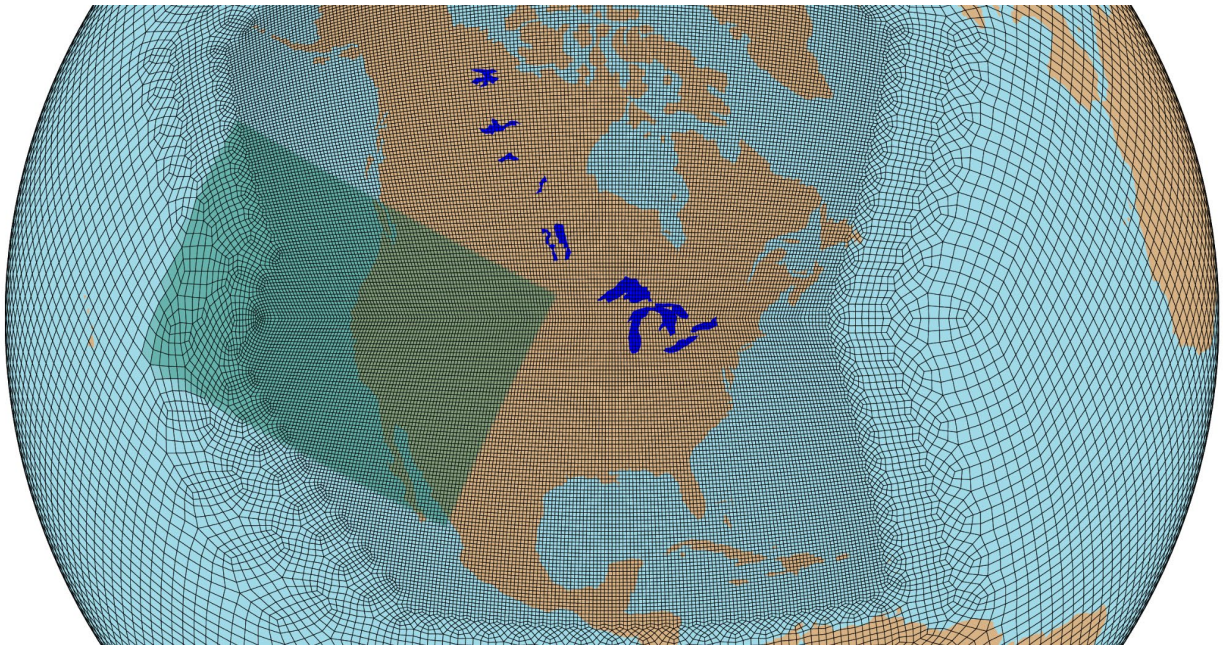

Figure 1. The regionally refined North American x4 grid used for regional simulations. The grid transitions from 1-degree grid spacing globally to 0.25-degree grid spacing over North America. The green overlay shows the region covered by the dynamically downscaled grid used for WRF simulations of the western U.S. (with grid spacing of 0.25 degree).

To ensure our analysis is sufficiently robust, the RRM and LRv2 simulations are conducted over the period 1985-2014 (30 years total). The DDM simulations use RRM data as forcing and also begin in 1985, but the first year is discarded, leaving 29 years for analysis.

TempestExtremes, a general-purpose and freely available feature detection and characterization software package, is used throughout this report to identify and characterize atmospheric rivers and heat waves (Ullrich et al. 2021).

Two metrics are used in this report for assessing agreement between model and reference. First, root mean square error (RMSE) is defined as

$$RMSE = \sqrt{\frac{\sum_i (o_i - p_i)^2 A_i}{\sum_i A_i}}$$

where o_i refers to the observed field in grid cell i, p_i refers to the model prediction, and A_i refers to the cell area. Second, index of agreement (IoA) complements RMSE, and is defined as

$$IoA = 1 - \frac{\sum_i (o_i - p_i)^2 A_i}{\sum_i \left(|p_i - \bar{o}| + |o_i - \bar{o}|\right)^2 A_i}$$

where the overline denotes the arithmetic mean. Values of IoA range from 0 to 1, with values closer to 1 indicating better agreement.

3.0 Results

3.1 Atmospheric Rivers

Atmospheric rivers are identified using the approach described in Ullrich et al. (2021): Grid points are first tagged as AR candidates when the smoothed Laplacian of the integrated vapor transport (IVT) falls below a prescribed threshold. Contiguous features smaller than 850,000 km^2 are then discarded. Only candidate grid points in the region bounded by [180W,100W] longitude and [20N,80N] latitude are retained for this study. For RRM and LRv2 simulations, detection is performed directly on the native grid. For the DDM simulation, data are superimposed atop the RRM simulation data prior to AR detection. This process is necessary because ARs are not gridpoint-local features but rely on information outside of the downscaling domain. In this section we assess several metrics related to ARs: frequency, wind speed at landfall, AR-related precipitation, and geometry.

Frequency

Figure 2 shows the annual frequency of ARs found in ERA5 reanalysis, along with the absolute difference in frequency between RRM, LRv2 and DDM simulations, and ERA5. Across all simulations, AR frequency is overestimated between California and Hawai'i. However, the use of higher resolution in RRM and DDM simulations over the eastern Pacific and western North America leads to substantial improvement in simulated AR frequency relative to LRv2. The dipole that appears in RRM and DDM simulations is indicative of a southward shift in the occurrence of ARs. Consistent with past analyses, Figure 3 shows that RRM and LRv2 simulations produce a mid-latitudinal jet that is shifted south relative to ERA5; given that ARs generally follow the large-scale circulation, this southward shift would drive a southward shift in AR occurrence.

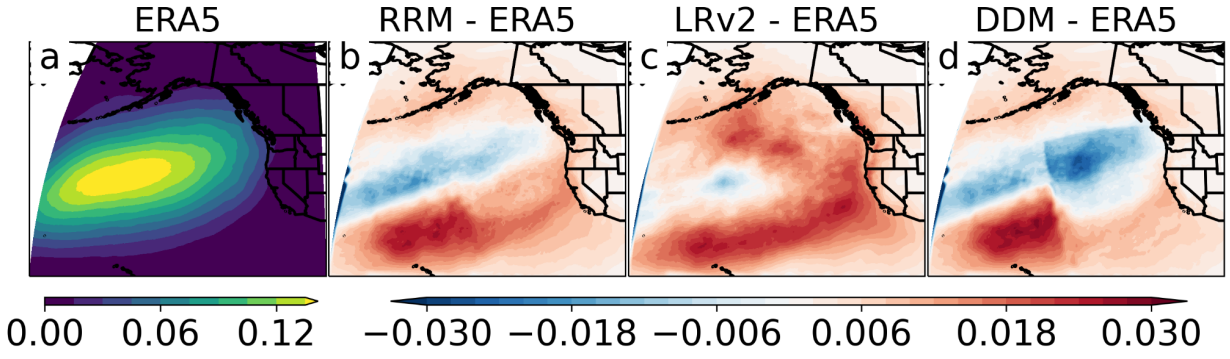

Figure 2. (a) Annual frequency of ARs in ERA5 reanalysis east of 180 degrees. Absolute difference in AR frequency between (b) RRM and ERA5, (c) LRv2 and ERA5, and (d) DDM and ERA5. The apparent discontinuity in (d) is due to the boundary of the downscaled grid.

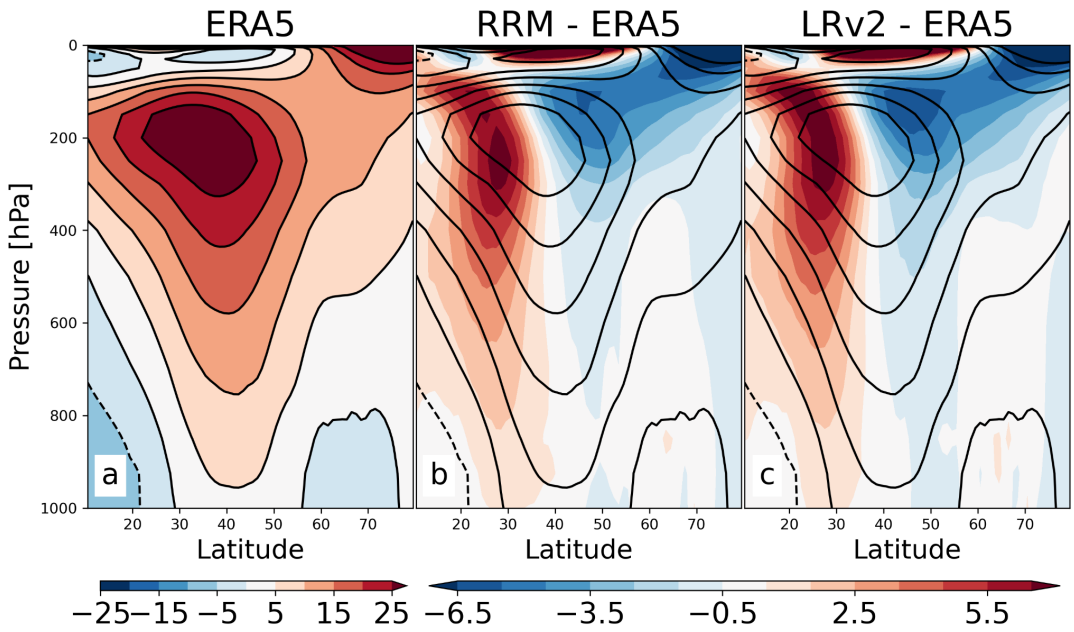

Figure 3. Zonal winds averaged over the Northern Pacific (180-110W) over November-March from (a) ERA5, and the differences between (b) RRM and ERA5 and (c) LRv2 and ERA5. The black contours in each panel are the contours from ERA5 climatology. Units are m/s.

Wind Speeds

Figure 4 shows histograms of AR wind speed from ERA5, RRM, LRv2, and DDM simulations accumulated over four coastal regions: the Pacific Northwest, Northern California, Central California and Southern California. All data sets have been regridded to 1 degree for fair comparison. There is striking qualitative agreement among all histograms, although the simulated wind speeds are consistently higher than in ERA5. This discrepancy should not necessarily be an indication of bias, as there is some evidence that ERA5 underestimates wind speeds in coastal regions (e.g., Gualtieri 2021).

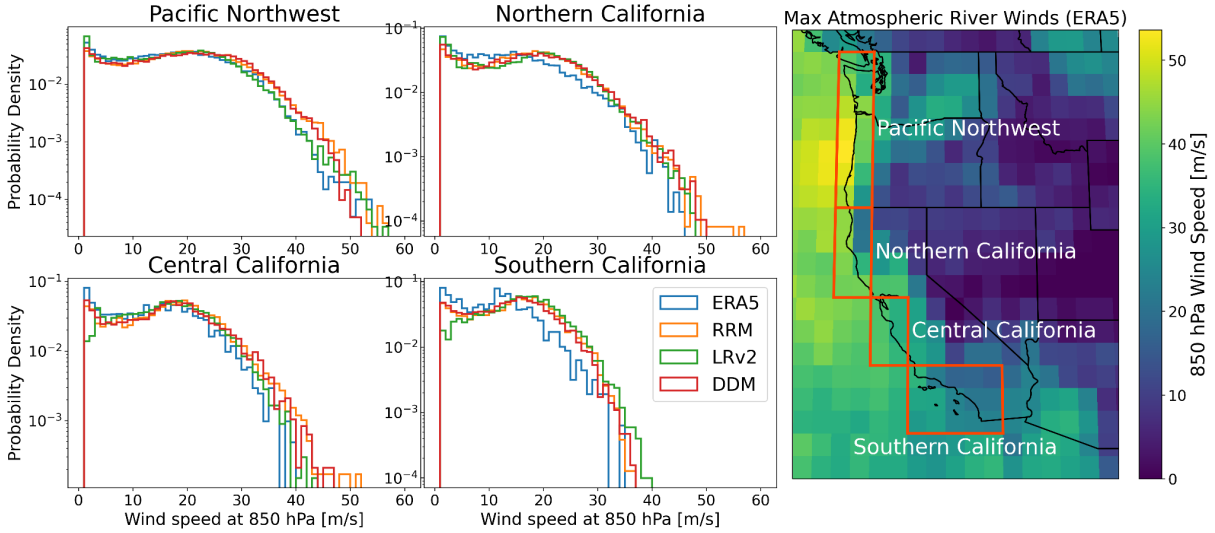

Figure 4. Histograms of AR wind speed in western U.S. coastal regions. Units are m/s.

Precipitation

Histograms of AR precipitation intensity from ERA5 (using NASA's Integrated Multi-satellite Retrievals for GPM [IMERG] precipitation), along with precipitation rates from model simulations, taken at 6 hourly frequency, are depicted in Figure 5 for the four regions delineated in Figure 4. IMERG precipitation is used here since it is an observational product, while ERA5 precipitation is diagnostic. The use of high resolution (either via RRM or DDM) leads to significantly better representation of precipitation intensity versus LRv2. Nonetheless, all products produce less-frequent intense precipitation in Northern California and the Pacific Northwest, where precipitation intensity sometimes exceeds 250 mm/day. Informed by these results, it is likely that even finer grid spacing over this region will lead to improvements in frequency of intense precipitation. Given that DDM also consistently yields higher precipitation intensities than RRM, it is likely that improvements in the microphysics parameterization of E3SM could also mitigate some of this bias.

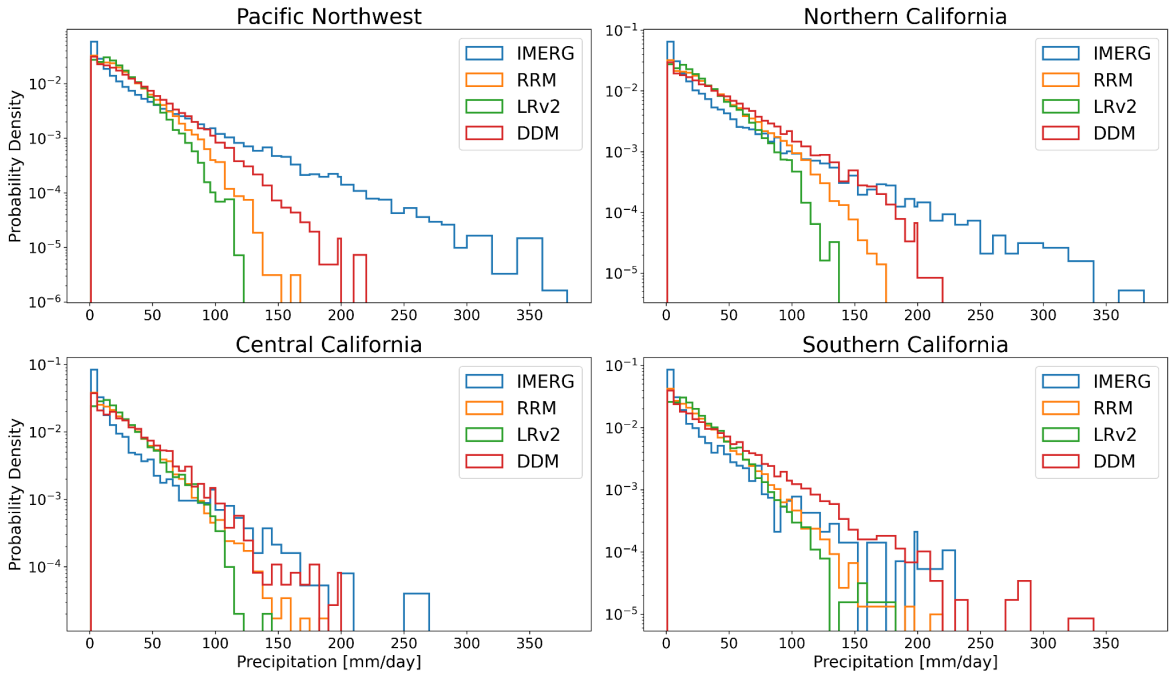

Figure 5. Histograms of precipitation associated with landfalling ARs. IMERG precipitation values are used (with ERA5 tracked AR objects) for observations. Units are mm/day.

Geometry

Geometric properties of AR objects detected by TempestExtremes, including centroid longitude, latitude, length, and width, are computed and depicted in Figure 6. AR centroids are computed by weighing the 3D Cartesian coordinate of each grid cell by integrated vapor transport, averaging over the AR object, then projecting the resulting coordinate to the surface of the sphere. AR length and width are computed using the principal component analysis approach of Inda-Díaz et al. (2021) but computed on the stereographic plane at the centroid coordinate of the AR object. Overall, there is broad consistency among data sets, except for the centroid latitude where ERA5 shows ARs concentrated in a narrower range of latitudes. This discrepancy is likely tied to the differences in jet position found in Figure 3.

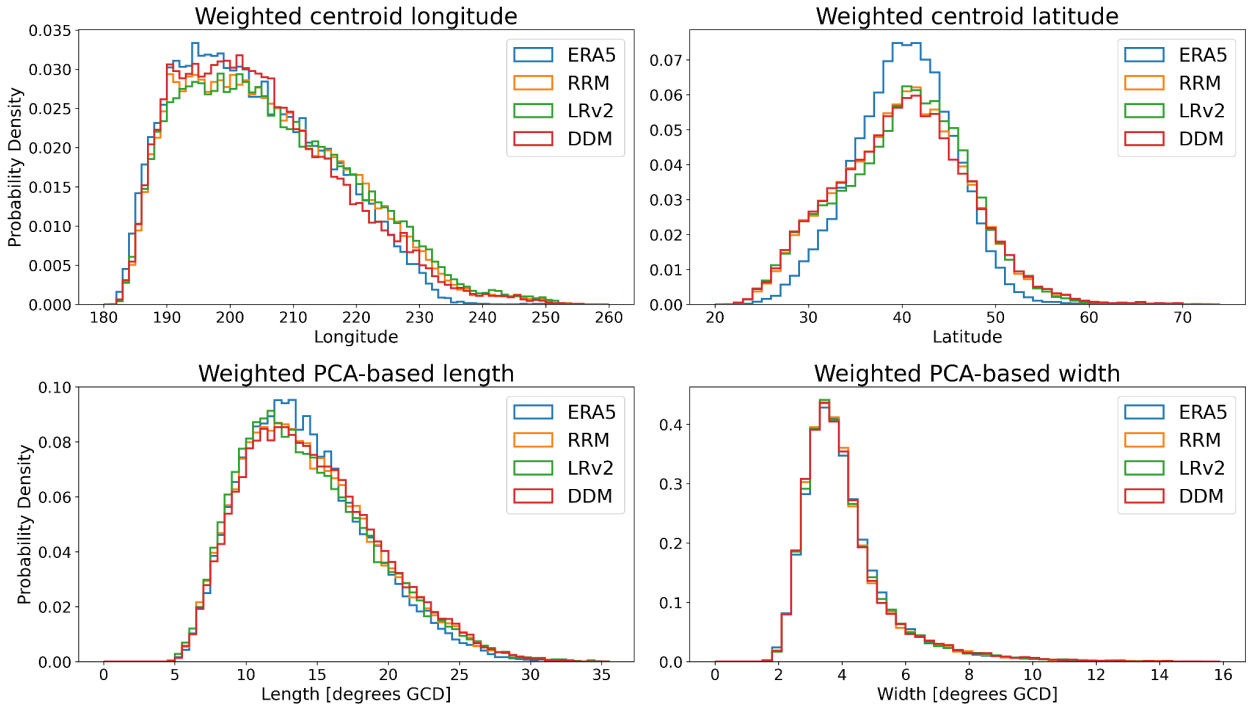

Figure 6. Histograms of AR geometry metrics, including centroid longitude and latitude, length, and width. Units are shown on each figure.

3.2 Heat Waves

Heat waves are also identified using TempestExtremes exclusively using data from the May-September period of each year. Grid points are tagged as having an active heat wave if at least two consecutive days record a maximum daily 2m temperature above the 95th percentile. In this section we examine four metrics related to heat waves: 95th percentile temperatures, event frequency, event intensity, and event duration.

95th Percentile Temperatures

Figure 7 shows the 95th percentile of May-September temperatures from ERA5, along with the differences between model simulations and ERA5. LRv2 does not resolve topography well, and hence there is significant imprinting in high-altitude regions and along the coastline. DDM is able to resolve topographic effects on temperature but tends to be biased cold relative to ERA5 and so does not show much improvement in RMSE over LRv2. RRM is also colder than ERA5 farther inland, but RMSE is significantly smaller in this model than in either LRv2 or DDM.

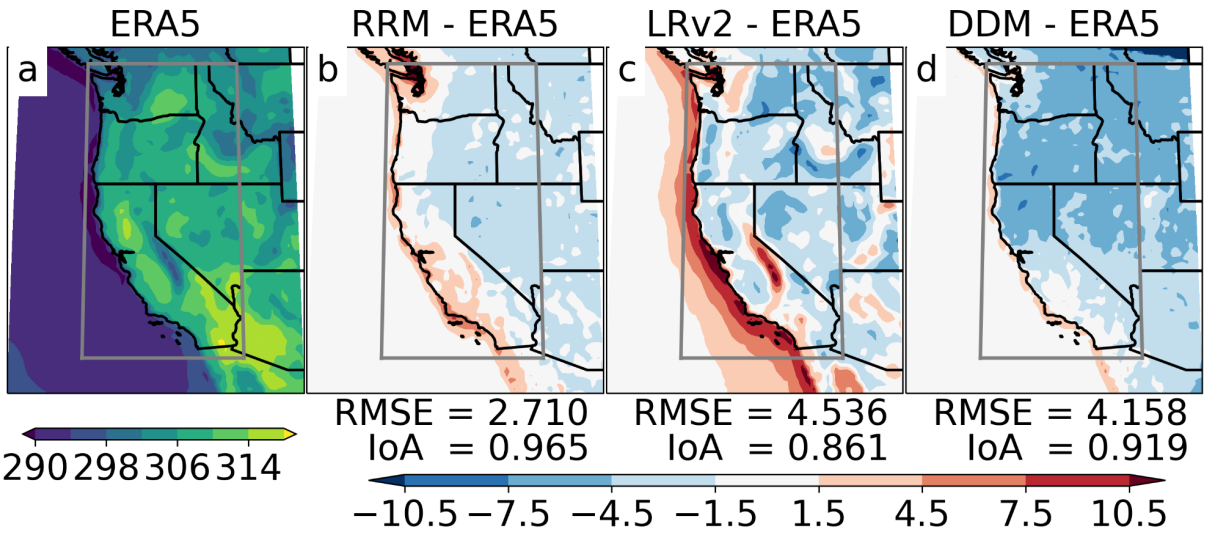

Figure 7. 95th percentile (May-September) 2m daily maximum temperature data from (a) ERA5, and the differences between (b) RRM and ERA5, (c) LRv2 and ERA5, and (d) DDM and ERA5. Units are K.

Frequency

Figure 8 is analogous to Figure 7 but shows average heat wave frequency (number of heat wave days per year). Errors are smallest with the RRM simulation, but both RRM and DDM simulations match well with ERA5 along the coast. The DDM simulation generally underestimates heat wave frequency inland, which suggests that DDM produces a few more days per year when temperatures above the 95th percentile do not persist for more than one day.

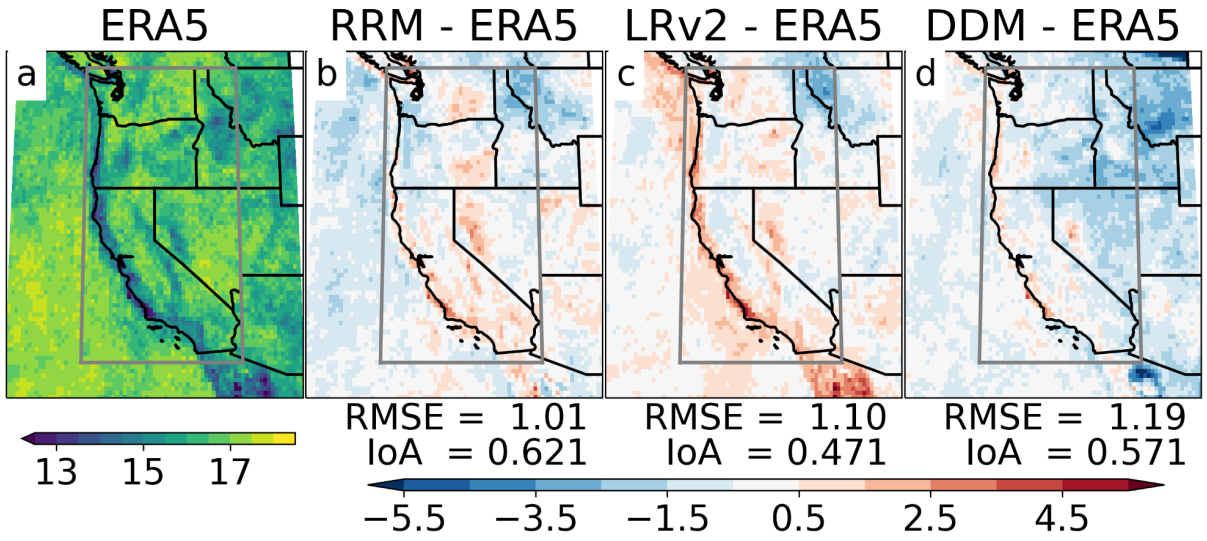

Figure 8. Average heat wave frequency (number of heat wave days per year) from (a) ERA5, and the differences between (b) RRM and ERA5, (c) LRv2 and ERA5, and (d) DDM and ERA5. Units are days.

Intensity

Figure 9 is analogous to Figure 7 but shows average heat wave intensity (average temperature during heat wave events minus 95th percentile temperature). All models generally produce warmer heat waves than in ERA5, except LRv2, which as a result of the coastal region being poorly resolved at low resolution, produces cooler temperature along the coast. Nonetheless, RMSE is relatively small and IoA is near 1, suggesting that all models generally capture intensity well.

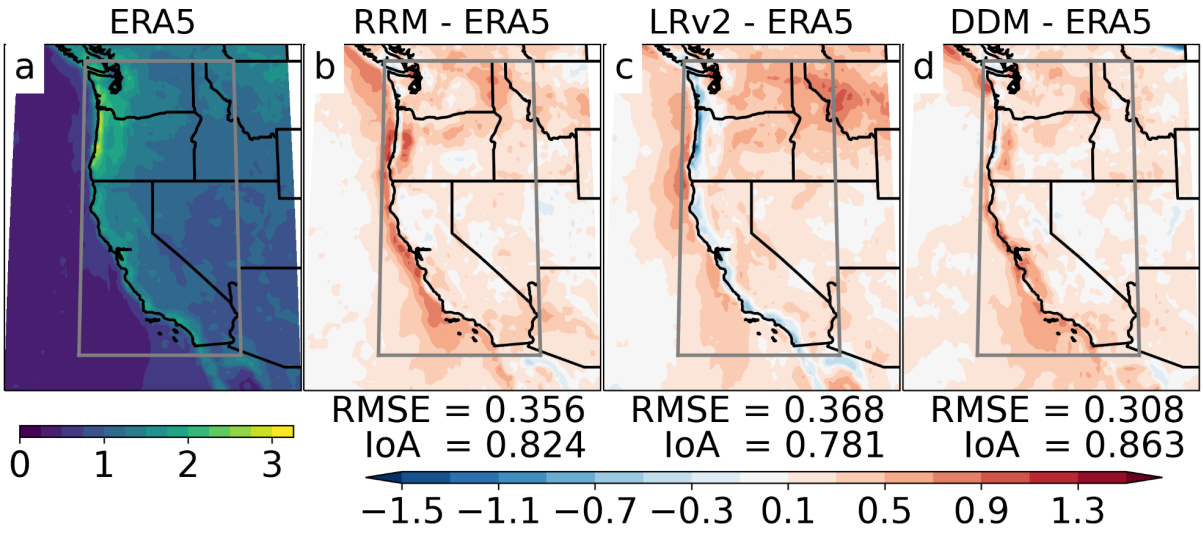

Figure 9. Average heat wave intensity (average temperature during heat wave events minus 95th percentile temperature) from (a) ERA5, and the differences between (b) RRM and ERA5, (c) LRv2 and ERA5, and (d) DDM and ERA5. Units are K.

Duration

Figure 10 is analogous to Figure 7 but shows average heat wave duration (number of days per heat wave event). Heat wave duration is a proxy for temporal autocorrelation in each grid cell; longer durations indicate warmer temperatures are generally more persistent. In all model simulations, heat wave duration is generally underestimated over the ocean and overestimated over land. All models have roughly equal RMSE and IoA, indicating that the higher resolution permitted by the RRM and DDM simulations does not improve this metric.

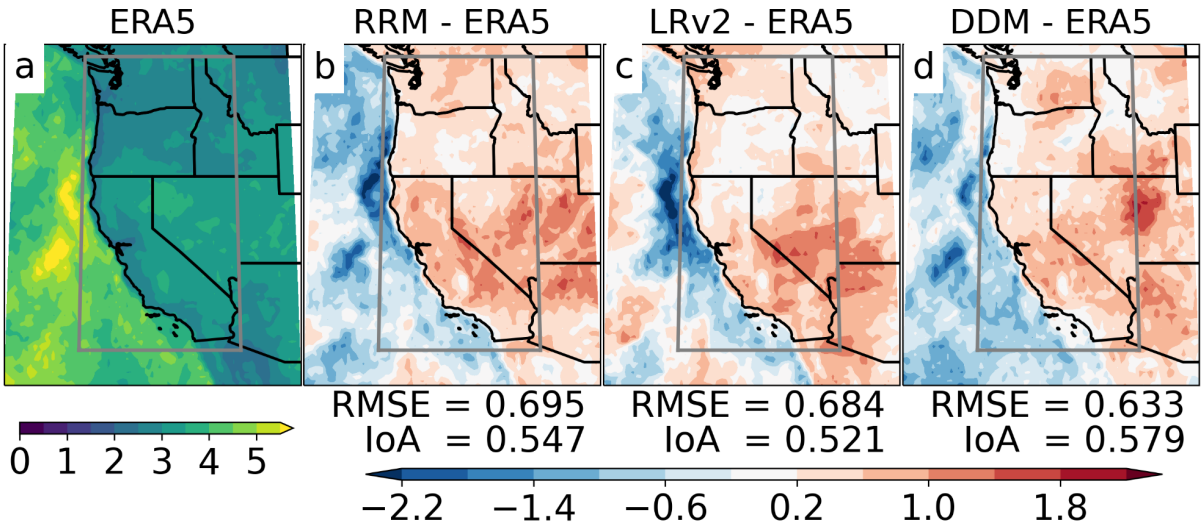

Figure 10. Average heat wave duration (number of days per heat wave event) from (a) ERA5, and the differences between (b) RRM and ERA5, (c) LRv2 and ERA5, and (d) DDM and ERA5. Units are days.

4.0 Summary

Results indicate that RRM and DDM over the region of interest produce clear improvements in AR frequency and landfalling AR precipitation, although a southward shift in AR location is apparent in all simulations relative to ERA5. Despite this improvement, AR precipitation intensity is weaker in the Pacific Northwest and Northern California relative to observations. Wind speeds in ARs and geometric characteristics of ARs are similar among all three configurations. For 95th percentile temperature, LRv2 does not accurately capture topographic variations in temperature. Both RRM and DDM capture topographic variation of temperatures correctly, but DDM produces a clear overland cold bias. HW frequency improves slightly in RRM, relative to LRv2, but is underestimated in DDM – nonetheless, differences across simulations are small. Both RRM and DDM improve on HW intensity, relative to LRv2, in large part because of better resolution of the coast. Among all simulations, HW duration is generally higher than ERA5 over land and lower than ERA5 over the ocean. In summary, although some AR and HW metrics are insensitive to grid spacing, many metrics improve in both RRM and DDM configurations.

A major accomplishment of this work is to demonstrate two novel capabilities: first, regional refinement in E3SMv2, which allows us to perform simulations with finer grid spacing in certain regions of interest; and second, the capability to dynamically downscale the regionally refined model. This latter technique is useful for assessing the performance of the two-way regionally refined model against more traditional dynamically downscaled models, while holding the meteorology of the coarse region fixed.

5.0 References

Chou, MD, and MJ Suarez. 1994. An efficient thermal infrared radiation parameterization for use in general circulation models. NASA Technical Memorandum 3: 104606.

Dennis, JM, J Edwards, KJ Evans, O Guba, PH Lauritzen, AA Mirin, A St-Cyr, MA Taylor, and PH Worley. 2012. "CAM-SE: A scalable spectral element dynamical core for the Community Atmosphere Model." *International Journal of High Performance Computing Applications* 26(1): 74−89, https://doi.org/10.1177/1094342011428142

Gent, PR, and JC Mcwilliams. 1990. "Isopycnal Mixing in Ocean Circulation Models." *Journal of Physical Oceanography* 20(1): 150−155, https://doi.org/10.1175/1520-0485(1990)020<0150:IMIOCM>2.0.CO;2

Gettelman, A, and H Morrison. 2015. "Advanced two-moment bulk microphysics for global models. Part I: Off-line tests and comparison with other schemes." *Journal of Climate* 28(3): 1268−1287, https://doi.org/10.1175/JCLI-D-14-00102.1

Gettelman, A, H Morrison, S Santos, P Bogenschutz, and PM Caldwell. 2015. "Advanced two-moment bulk microphysics for global models. Part II: Global model solutions and aerosol-cloud interactions." *Journal of Climate* 28(3): 1288−1307, https://doi.org/10.1175/JCLI-D-14-00103.1

Golaz, J-C, VE Larson, and WR Cotton. 2002. "A PDF-Based Model for Boundary Layer Clouds. Part I: Method and Model Description." *Journal of the Atmospheric Sciences* 59(24): 3540−3551, https://doi.org/10.1175/1520-0469(2002)059<3540:APBMFB>2.0.CO;2

Gualtieri, G. 2021. "Reliability of ERA5 reanalysis data for wind resource assessment: a comparison against tall towers." *Energies* 14(14): 4169, https://doi.org/10.3390/en14144169

Hersbach, H, B Bell, P Berrisford, S Hirahara, A Horányi, J Muñoz-Sabater, J Nicolas, C Peubey, R Radu, D Schepers, and A Simmons. 2020. "The ERA5 global reanalysis." *Quarterly Journal of the Royal Meteorological Society* 146(730): 1999−2049, https://doi.org/10.1002/qj.3803

Hong, SY, J Dudhia, and SH Chen. 2004. "A revised approach to ice microphysical processes for the bulk parameterization of clouds and precipitation." *Monthly Weather Review* 132(1): 103−120, https://doi.org/10.1175/1520-0493(2004)132<0103:ARATIM>2.0.CO;2

Iacono, MJ, JS Delamere, EJ Mlawer, MW Shephard, SA Clough, and WD Collins. 2008. "Radiative forcing by long-lived greenhouse gases: Calculations with the AER radiative transfer models." *Journal of Geophysical Research – Atmospheres* 113(D13): D13103, https://doi.org/10.1029/2008JD009944

Inda-Díaz, HA, TA O'Brien, Y Zhou, and WD Collins. 2021. "Constraining and Characterizing the Size of Atmospheric Rivers: A Perspective Independent from the Detection Algorithm." *Journal of Geophysical Research − Atmospheres* 126(16): e2020JD033746, https://doi.org/10.1029/2020JD033746

Janjić, ZI. 1994. "The step-mountain eta coordinate model: Further developments of the convection, viscous sublayer, and turbulence closure schemes." *Monthly Weather Review* 122(5): 927−945, https://doi.org/10.1175/1520-0493(1994)122<0927:TSMECM>2.0.CO;2

Kain, JS. 2004. "The Kain–Fritsch convective parameterization: an update." *Journal of Applied Meteorology and Climatology* 43(1): 170−181, https://doi.org/10.1175/1520-0450(2004)043<0170:TKCPAU>2.0.CO;2

Larson, VE, and J-C Golaz. 2005. "Using Probability Density Functions to Derive Consistent Closure Relationships among Higher-Order Moments." *Monthly Weather Review* 133(4): 1023−1042, https://doi.org/10.1175/MWR2902.1

Li, H, MS Wigmosta, H Wu, M Huang, Y Ke, AM Coleman, and LR Leung. 2013. "A physically based runoff routing model for land surface and earth system models." *Journal of Hydrometeorology* 14(3): 808−828, https://doi.org/10.1175/JHM-D-12-015.1

Li, HY, LR Leung, A Getirana, M Huang, H Wu, Y Xu, J Guo, and N Voisin. 2015. "Evaluating global streamflow simulations by a physically based routing model coupled with the community land model." *Journal of Hydrometeorology* 16(2): 948−971, https://doi.org/10.1175/JHM-D-14-0079.1

Liu, X, P-L Ma, H Wang, S Tilmes, B Singh, RC Easter, SJ Ghan, and PJ Rasch. 2016. "Description and evaluation of a new four-mode version of the Modal Aerosol Module (MAM4) within version 5.3 of the Community Atmosphere Model." *Geoscientific Model Development* 9(2): 505−522, https://doi.org/10.5194/gmd-9-505-2016

Mlawer, EJ, SJ Taubman, PD Brown, MJ Iacono, and SA Clough. 1997. "Radiative transfer for inhomogeneous atmospheres: RRTM, a validated correlated-k model for the longwave." *Journal of Geophysical Research – Atmospheres* 102(D14): 16663−16682, https://doi.org/10.1029/97JD00237

Neale, RB, JH Richter, and M Jochum. 2008. "The impact of convection on ENSO: From a delayed oscillator to a series of events." *Journal of Climate* 21(22): 5904-5924, https://doi.org/10.1175/2008JCL12244.1

Niu, GY, ZL Yang, KE Mitchell, F Chen, MB Ek, M Barlage, A Kumar, K Manning, D Niyogi, E Rosero, and M Tewari. 2011. "The community Noah land surface model with multiparameterization options (Noah-MP): 1. Model description and evaluation with local-scale measurements." *Journal of Geophysical Research − Atmospheres* 116(D12): D12109, https://doi.org/10.1029/2010JD015140

Oleson, KW, DM Lawrence, GB Bonan, B Drewniak, M Huang, CD Koven, S Levis, F Li, WJ Riley, ZM Subin, SC Swenson, PE Thornton, A Bozbiyik, R Fisher, CL Heald, E Kluzek, J-F Lamarque, PJ Lawrence, LR Leung, W Lipscomb, S Muszala, DM Ricciuto, W Sacks, Y Sun, J Tang, and Z-LYang. 2013. Technical description of version 4.5 of the Community Land Model (CLM). NCAR/TN-478+STR, https://doi.org/10.5065/D6RR1W7M

Petersen, MR, XS Asay-Davis, AS Berres, Q Chen, N Feige, MJ Hoffman, DW Jacobsen, PW Jones, ME Maltrud, SF Price, TD Ringler, GJ Streletz, AK Turner, LP Van Roekel, M Veneziani, JD Wolfe, PJ Wolfram, and JL Woodring. 2019. "An Evaluation of the Ocean and Sea Ice Climate of E3SM Using MPAS and Interannual CORE-II Forcing." *Journal of Advances in Modeling Earth Systems* 11(5): 1438−1458, https://doi.org/10.1029/2018MS001373

Rasch, PJ, S Xie, P-L Ma, W Lin, H Wang, Q Tang, SM Burrows, P Caldwell, K Zhang, RC Easter, P Cameron-Smith, B Singh, H Wan, JC Golaz, BE Harrop, E Roesler, J Bacmeister, VE Larson, KJ Evans, Y Qian, M Taylor, LR Leung, Y Zhang, L Brent, M Branstetter, C Hannay, S Mahajan, A Mametjanov, R Neale, JH Richter, J-H Hoon, CS Zender, D Bader, M Flanner, JG Foucar, R Jacob, N Keen, SA Klein, X Liu, AG Salinger, M Shrivastava, and Y Yang. 2019. "An Overview of the Atmospheric Component of the Energy Exascale Earth System Model." *Journal of Advances in Modeling Earth Systems* 11(8): 2377−2411, https://doi.org/10.1029/2019MS001629

Richter, JH, and PJ Rasch. 2008. "Effects of convective Momentum Transport on the Atmospheric Circulation in the Community Atmosphere Model, Version 3." *Journal of Climate* 21(7): 1487−1499, https://doi.org/10.1175/2007JCLI1789.1

Ringler, T, M Petersen, RL Higdon, D Jacobsen, PW Jones, and M Maltrud. 2013. "A multi-resolution approach to global ocean modeling." *Ocean Modelling* 69: 211−232, https://doi.org/10.1016/j.ocemod.2013.04.010

Skamarock, WC, JB Klemp, J Dudhia, DO Gill, D Barker, MG Duda, X-Y Huang, W Wang, and JG Powers. 2008. A description of the advanced research WRF version 3. NCAR/TN-475+STR, https://doi.org/10.5065/D68S4MVH

Subin, ZM, WJ Riley, and D Mironov. 2012. "An improved lake model for climate simulations: Model structure, evaluation, and sensitivity analyses in CESM1." *Journal of Advances in Modeling Earth Systems* 4(1): M02001, https://doi.org/10.1029/2011MS000072

Taylor, MA, O Guba, A Steyer, PA Ullrich, DM Hall, and C Eldred. 2020. "An energy consistent discretization of the nonhydrostatic equations in primitive variables." *Journal of Advances in Modeling Earth Systems* 12(1): e2019MS001783, https://doi.org/10.1029/2019MS001783

Ullrich, PA, CM Zarzycki, EE McClenny, MC Pinheiro, AM Stansfield, and KA Reed. 2021. "TempestExtremes v2. 1: A community framework for feature detection, tracking, and analysis in large datasets." *Geoscientific Model Development* 14(8): 5023−5048, https://doi.org/10.5194/gmd-14-5023-2021

Wang, H, RC Easter, R Zhang, P-L Ma, B Singh, K Zhang, D Ganguly, PJ Rasch, SM Burrows, SJ Ghan, S Lou, Y Qian, Y Yang, Y Feng, M Flanner, LR Leung, X Liu, M Shrivastava, J Sun, Q Tang, S Xie, and J-H Yoon. 2020. "Aerosols in the E3SM Version 1: New developments and their impacts on radiative forcing." *Journal of Advances in Modeling Earth Systems* 12(1): e2019MS001851, https://doi.org/10.1029/MS001851

Zhang, GJ, and NA McFarlane. 1995. "Sensitivity of climate simulations to the parameterization of cumulus convection in the Canadian climate centre general circulation model." *Atmosphere-Ocean* 33(3): 407−446, https://doi.org/10.1080/07055900.1995.9649539

U.S. DEPARTMENT OF
ENERGY

Office of Science